63rd International Astronautical Congress, Naples, Italy. Copyright 2012 by Dr. Massimiliano Vasile. Published by the IAF, with permission and released to the IAF to publish in all forms..

IAC-12.C3.1.5

FRACTIONATED SOLAR POWER SATELLITE FOR REGIONAL COVERAGE

Massimiliano Vasile
Department of Mechanical and Aerospace Engineering, University of Strathclyde, United Kingdom,
massimiliano.vasile@strath.ac.uk

This paper presents a preliminary analysis of a fractionated solar power satellite system for regional coverage. The fractionated system is composed of a cluster of satellites, in different possible configurations, that concurrently beam energy to the ground through medium power lasers. The paper presents an analysis of the possible orbit solutions that can be adopted to provide power during the night time to local users in different regions of the world. The system is intended to serve mobile stations or local stations that can be hardly accessed by normal power lines or are cut off during disasters. A preliminary system analysis shows that with a limited number of small size satellite local users can be provided with a few kWh of energy every day.

Keywords: solar power satellite, fractionated satellites, frozen orbits, heliotropic orbits, sun-synchronous orbits, formation flying, laser wireless power transmission.

I. INTRODUCTION

Typical Solar Power Satellite (SPS) architectures, in the reference literature, envisage large structures in space delivering MWatt to GWatt of power from geosynchronous orbit (GEO)[1,2]. In the past SPS infrastructures were monolithic but recent advances propose modular architecture with an incremental assembling process[3]. Yet even with these new architectural schemes, the final result is still a large infrastructure delivering high power levels from GEO to a single stationary user. This paper presents a preliminary analysis of a fractionated architecture for a solar power satellite (FSPS) designed to deliver power to local ground users in remote areas. The fractionated SPS architecture is based on either a formation of small satellites, each equipped with a laser system and deployable arrays, or by a single master spacecraft generating power and a number of slave satellites beaming power to the ground. The output power considered from each spacecraft ranges from few hundred Watts to few kW.

The concept is derived from an analogous system for asteroid deflection with laser ablation[4]. The satellites in the formation would continuously beam power onto a designed spot on the surface of the Earth to provide a total of a few hundreds to a few thousands Watts level of power to disaster regions, military camps or users in remote areas. One advantage of a fractionated architecture is that some systems are not completely scalable (laser, thermal control, power distribution and control) and might require specific technology developments if high level of power outputs are needed from a single spacecraft.

The paper presents an analysis of different possible orbits and formation configurations for a fractionated SPS system. A number potentially interesting existing orbital solutions will be considered ranging from standard Sun-synchronous low altitude orbits, to Molniya orbits, to heliotropic orbits[10,11,12].

A preliminary system analysis is presented to better understand both which types of services this system can deliver, and to which needs, user or otherwise, it can address. In particular, the number and size of the spacecraft, level of power installed on board of each spacecraft and ground coverage will be considered in the system analysis.

II. SPACECRAFT CONCEPTUAL DESIGN

We will consider three different configurations for the disaggregated system: a) close formation of homogenous spacecraft, b) master-slave laser configuration, c) master-slave near-field configuration. The three configurations are represented in Figure 1, Figure 2 and Figure 3 respectively.

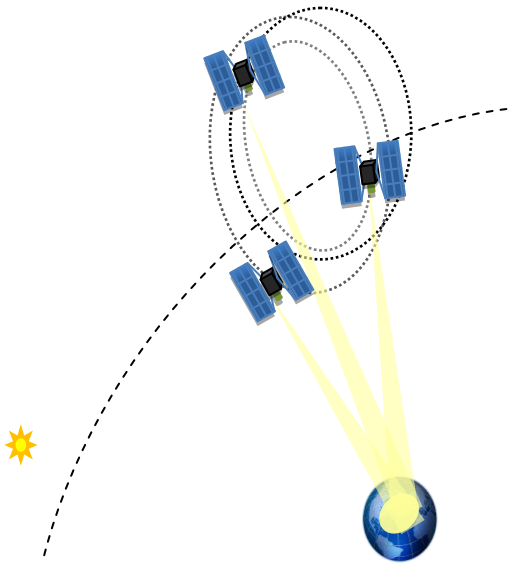

Figure 1. Homogenous cluster

In the homogenous cluster architecture all the spacecraft have an identical mass and configuration, all carrying a laser beam and a power system. The spacecraft fly in formation and collectively beam energy to the same receiver. In the master-slave laser configuration, the master generates all the laser beams and the slaves simply redirect and collimate the beams to the ground receiver. Finally, in the master-slave near-field configuration, the master generates the near field, the slaves each generate one laser beam and all the laser beams are collimated to the same ground station.

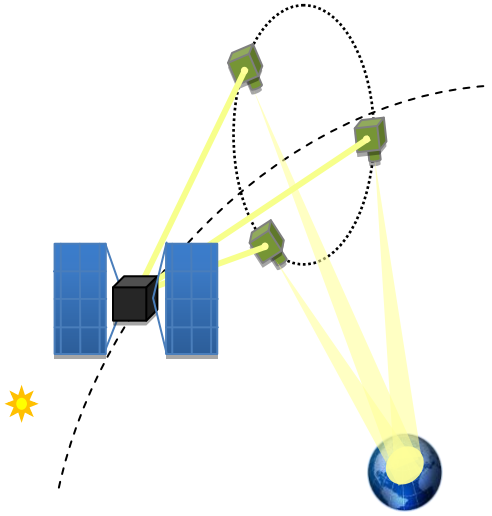

Figure 2. Master-slave laser cluster

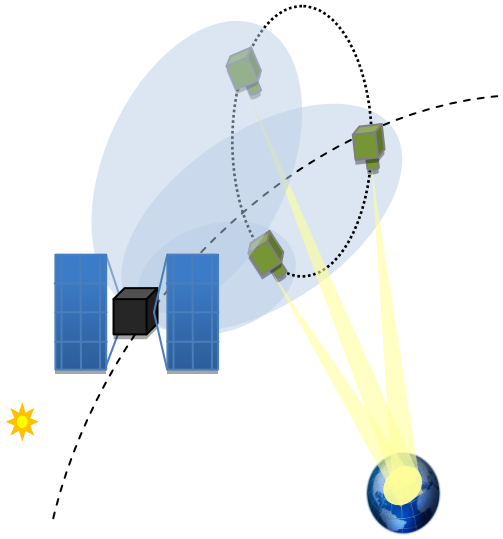

Figure 3. Master-slave near-field cluster

II.I Beam Quality Considerations

The power delivered to the ground and the size of the receiver depends on the quality of the beam, and its propagation through space and the atmosphere.

One can reasonable assume that the beam is Gaussian, therefore the cross-section radius of the beam is given by:

$$w = w_0\sqrt{1+\left(\frac{z}{z_R}\right)^2} \quad [1]$$

with the Rayleigh range given by:

$$z_R = \frac{\pi w_0^2}{\lambda} \quad [2]$$

with wavelength λ. We assume here to have either a beam expander or a focusing mirror on the spacecraft beaming energy down to Earth. In the case of a beam expander the magnification of the waist radius w_0 is given by:

$$m = \frac{w_0^m}{w_0} = \frac{1}{\sqrt{\left(1-\frac{s}{f}\right)^2+\left(\frac{z_R}{f}\right)^2}} \quad [3]$$

with f the focal length of the focusing lens, s the distance of the waist w_0 from the lens and $w_0{}^m$ the post magnification waist radius. The post magnification Rayleigh range becomes:

$$z_R^m = m^2 z_R \quad [4]$$

Due to the low power level of each beam, the atmosphere is not expected to offer a self-focusing effect as demonstrated in Rubenchick et al.[7]. Instead it is expected that the atmosphere will attenuate the incoming beam according to the Beers-Lambert law:

$$P_r = P_e e^{-\sigma h_A} \quad [5]$$

with P_e the emitted power, P_r the received power, h_A the thickness of the atmosphere and σ given by[6]:

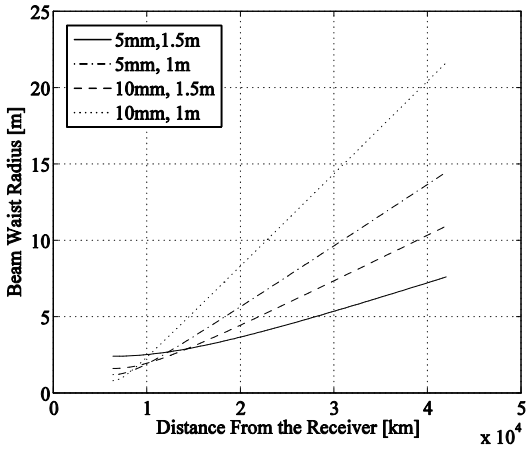

Figure 4. Beam waist radius as a function of the distance from the receiver for different beam expanders.

$$\sigma = \frac{3.91}{h_V}\left(\frac{\lambda}{550}\right)^{-q} \quad [6]$$

where h_v is the maximum visibility (in km) and q = 1.6 is the size distribution of the scattering particles which for high visibility (> 50 km).

Figure 4 shows the variation of the radius of the spot on the ground as a function of the distance of the receiver from the emitter. The assumption is that the beam expander is made of a series of three lenses, the first two with a focal distance of 5-10 mm and the last one with a focal distance of 1-1.5 m. The first lens is placed at distance s = 0 from the laser output and the last lens at a distance $s = f$ from the intermediate lens. From Figure 4 one can see that for small and easily portable receivers, the maximum distance should remain limited below 25000 km.

II.II System Design Considerations

From Eqs. [5] and [6] one can see that, even in the case of high visibility, the power received on the ground is about 46% of the power entering the atmosphere for an eye safe frequency of 1520 nm. This poses immediately an initial concern due to the dissipation of energy into the atmosphere. The second concern is the amount of power that can actually be delivered on ground. This latter concern is the driving parameter for the sizing of the space segment. The current assumption is to provide a few kWh to a mobile station or fixed base during night time, therefore the power received can be from few hundred Watts to a kW depending on the beaming time. The power conversion efficiency at the receiver is assumed to be 60% because the wavelength of the light is supposed to be matched to the band gap of the solar cells. Therefore, a 1 kW laser output would generate about 276 W at the receiver.

The laser system on board the spacecraft is composed of a laser diode coupled to a fibre plus collimating optics. From recent developments supported by DARPA and realised by nLIGHT[15], laser diodes have been demonstrated with an 80% efficiency or higher with output power for a single element of up to 350 W, with stacks going up to few kW[16]. In particular, experimental results have demonstrated wall-plug efficiencies of about 83% at 138 K and 76% at 283 K. Cryogenic temperature can represent a serious challenge especially over long periods of time. A laser system operating at temperatures between 273 K and 283 K seems more reasonable and poses less demanding constraints on the thermal control system. The beam quality of these laser diodes is not high enough to produce the right power density. These laser diodes can instead pump fibres that, at present, have already reached an 83% optical-to-optical efficiency[17,18]. The coupling between fibres and laser diode requires some attention but efficiencies between 80-90% are achievable. It is therefore reasonable to expect a diode+fibre coupling with an overall efficiency between 50% and 57% with the possibility to increase the overall efficiency to 62% by further cooling the laser. Heat rejection is required at two stages: at diode level and then at fibre level. Assuming, for example, a 1 kW output power the required heat rejection at diode level is between 200 W to 240 W while at fibre level is between 130 W and 136 W. An alternative to the use of fibres coupled with laser diodes is to employ direct solar pumping using concentrators and semiconductor disks[20]. However, at present, directly pumped lasers demonstrate relatively low efficiencies, below 10%, with the exception of recent lab experiments that demonstrated very high efficiencies but at very low power. This technology is considered to be less mature than a fibre+diode solution but could be a valid solution to significantly cutting down the mass and cost of the power system required to manage an indirectly pumped laser. A review of lasers solutions for wireless power transmission can be found in Summerer et al. [5].

The thermal control system of the laser is assumed to be fully passive. The laser is mounted inside a turret which flanges to radiate the excess power. The assumption of a purely passive system can be retained if the rejected power is limited to a few hundred Watts to a few kWatts. For higher rejections, a different system might be necessary. This imposes a limit on the size of the master spacecraft for the master-slave laser cluster configuration. In order to evaluate the size of the radiators (flanges) for the laser assembly, one can assume a steady state rejection through radiation by solving the simple equation:

$$\sigma\varepsilon_R A_R T_R^4 = Q_{RL} \quad [7]$$

in which the temperature of the radiator T_R is lower than the required temperature of the laser, Q_{RL} is the power to be rejected, ε_R=0.95 the emissivity of the radiator and A_R its area. The laser assembly, considering the diode rack, collimator and fibres has limited mass, while the associated thermal control system represent the bulk of the mass of the laser system. The mass of the radiators is taken to be 4 kg/m^2 while the mass of the laser assembly is assumed to be 1 kg per laser assembly with each laser assembly delivering up to 1 kW of output power. In the homogenous cluster configuration, each spacecraft would support one laser assembly with associated radiators while in the master-slave configuration all the lasers are on the master. Given the overall efficiency of a coupled diode-fibre system, the input to the laser for a 1 kW power output should be 2 kW which translates into 6.3 m^2 of solar arrays assuming a cell efficiency of 0.3, with an assembly degradation of 0.9 and a power system conversion efficiency of 0.85. In the master-slave configuration, the master illuminates each slave with one laser beam. The

slave satellite simply redirects the incoming beam toward the beam expander and ultimately towards Earth. The main power losses are due to the multiple reflections and to the beam expander. If one assumes a 97% reflectivity and a single reflection at the slave satellite, the master-slave configuration has to include a further 3% degradation of the beamed power compared to a homogenous cluster. The sizing of the spacecraft follows the figures and percentages in Table 1, taken from historical data and reference books[21]. The payload is the laser assembly plus the beam expander. The beam expander is essentially a 1.5 m long telescope, and the conservative assumption here is that its mass is equivalent to the one of the Mars Reconnaissance Orbiter high resolution telescopes, which is 65 kg. A single spacecraft in the homogenous formation, therefore, would have a dry mass of 275 kg including a 20% system margin, with an area to mass ratio of 0.02 m^2/kg and solar pressure perturbation of 1e-7 m/s^2. In the master-slave configuration, the master would not support any beam expander but would carry all the lasers with associated heat rejection systems. The slaves would have a dry mass of 150 kg and the master a mass of 140 kg per each slave satellite in the formation. As a result, for each kW of power generated at the receiver, the homogenous cluster would have a dry mass in orbit of 1100 kg while the master-slave cluster would have a mass of 1160 kg. The area to mas ratio of the master would be 0.046 with a solar pressure acceleration of 2.1e-7 m/s^2. If the mass of the beam expander is significantly reduced the homogenous cluster becomes quite attractive though with less pointing flexibility.

Table 1. Spacecraft subsystems mass breakdown

Item	Mass
AOCS	10.0% of dry mass
Electric Propulsion	27.1 kg
Data Handling and Comms	8% of dry mass
Power	20 kg/kW
Structure	18% of dry mass
Harness	6.0% of dry mass

For the near-field cluster configuration, one can assume that each slave spacecraft is essentially equivalent to the homogenous one as it has to support the laser system plus the beam expander. The power system is different[13] but it can be assumed to have comparable mass as the driving mass is probably the power conversion and processing unit. The master does not support the laser and associated heat rejection system but needs a power system and the set of coils to generate the near field. A variant to the master-slave laser configuration would employ a master satellite that directly concentrate the sun light onto the slave satellites by using reflectors. This last configuration is expected to be equivalent to the near-field configuration though the master is expected to have a much higher area to mass ratio than the slave satellites and therefore it would be subject to a higher solar pressure perturbation.

III. ORBIT ANALYSIS

One can consider a variety of possible orbits. The goal is to serve multiple users or a single user multiple times within a single day. One can distinguish between two types of users: a mobile user and a fixed station. The former user needs a moving ground-track or flexible beam steering capabilities while the latter requires a ground-track repeating solution.

A further requirement is to serve the user at particular times during the day. Here it will be considered the case in which power is mainly required during the night to minimise energy storage and allow operations when ground installed solar arrays are not working. This last requirement implies a sun-following or sun-synchronous solution. Such a solution would also allow an ideal illumination condition of the satellites in orbit with minimum attitude and reconfiguration requirements.

The analysis of sun-synchronous solutions can start by taking the secular variation of the line of the nodes and the line of the apsis due to J_2, the oblateness of the Earth. In this paper we will limit the analysis to the gravitational effects only and considering only J_2 however a complete treatment would require including higher harmonic terms and solar pressure. This analysis therefore represents a first indication of possible solution for the disaggregated SPS system. The secular variations of the right ascension of the ascending node and the argument of the perigee due to J_2 can be written as[9]:

$$\dot{\Omega} = -\frac{3nR_E^2 J_2}{2p^2}\cos i \qquad [8]$$

$$\dot{\omega} = \frac{3nR_E^2 J_2}{4p^2}\left(4-5\sin^2 i\right) \qquad [9]$$

By combining Eqs. [8] and [9] one can impose the simple sun-synchronicity condition:

$$\Delta_{SS} = \frac{3nR_E^2 J_2}{4p^2}\left(4-5\sin^2 i\right) - \frac{3nR_E^2 J_2}{2p^2}\cos i - \frac{2\pi}{P_E} = 0 \qquad [10]$$

Eq. [10] is valid for prograde orbits, i.e., with an inclination from 0^o to 90^o. For retrograde orbits, the helio-synchronicity condition reads:

$$\Delta_{SS} = -\frac{3nR_E^2 J_2}{4p^2}\left(4-5\sin^2 i\right) - \frac{3nR_E^2 J_2}{2p^2}\cos i - \frac{2\pi}{P_E} = 0 \qquad [11]$$

In the following, the term heliotropic, proposed by Hedman et al.[11] and Colombo et al.[12] will be used to identify orbits that satisfy conditions [10] or [11].

If a repeated ground track is required then one has to compute the correction to the orbital period due to the drift in the argument of the periapsis and the mean motion given by[9]:

$$P_{\Omega} = P_n \left(1 + \frac{3nJ_2}{4} \left(\frac{R_E}{p} \right)^2 \left(-\sqrt{1-e^2}(2-3\sin^2 i) + 4 - 5\sin^2 i \right) \right)^{-1} \quad [12]$$

The corrected period needs to be equal to the period in which a subsatellite revisits a station including the drift in right ascension of the ascending node:

$$P_{GT} = \frac{2\pi}{\omega_E - \dot{\Omega}} \quad [13]$$

which gives the repeated-ground track condition:

$$P_{\Omega} = \frac{k}{j} P_{GT} \quad [14]$$

where k and j are two integer numbers. Figure 5 shows the level curves of Δ_{SS} for different inclinations and altitude of the apogee assuming a constant perigee at an altitude of 600 km. The red curves correspond to $\Delta_{SS} = 0$. The almost vertical brown lines are the solutions of Eq. [14] with (from left to right) the following resonances:

$$k/j \in \{1/10,\ 1/8,\ 1/6,\ 1/5\},$$

the intersection between the resonance curves and red lines give the heliotropic repeated ground track solutions. For example, if a solution along the red line has a resonance 1/5 it means that the station on the Earth can see a satellite at the zenith every 5 orbits. Figure 5 also shows that, as expected, heliotropic Molniya orbits with an inclination of 63.5° are not possible. On the other hand, prograde solutions below 40° are possible with a maximum altitude between 20000 km and 25000 km. Lastly, the figure shows the classical circular sun-synchronous solutions at about 95° inclination and a family of retrograde orbits.

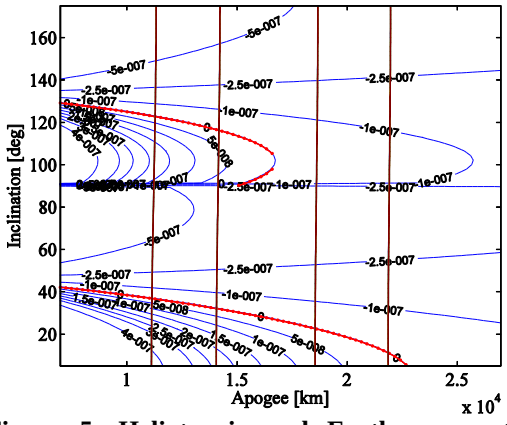

Figure 5. Heliotropic and Earth resonant solutions for a perigee altitude of 600 km.

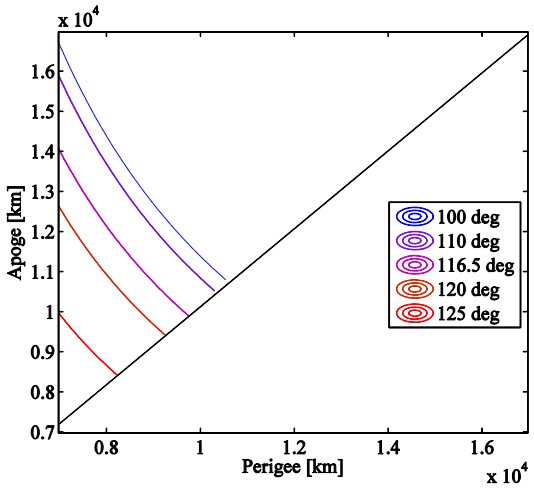

Figure 6. Heliotropic retrograde solutions for different inclinations and apogee, perigee radii.

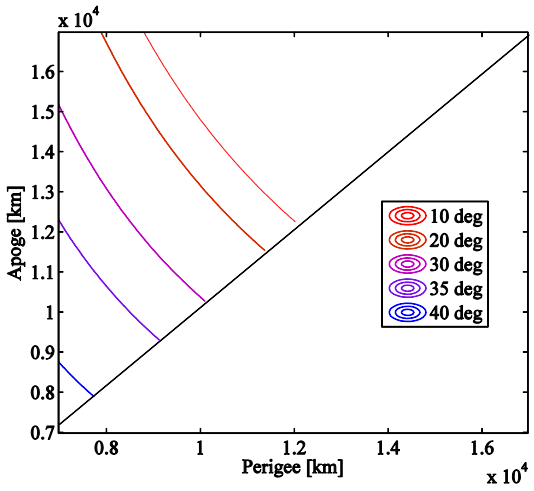

Figure 7. Heliotropic prograde solutions for different inclinations and apogee, perigee radii

If the perigee is free, one can look for heliotropic solutions at different inclinations for a variable perigee and apogee radius. The result can be seen in Figure 6 and Figure 7 for retrograde and prograde solutions respectively. Figure 6 in particular shows that retrograde heliotropic solutions at the critical inclination are possible though with a limited semi-major axis (giving a short period)[19].

A high altitude of the apogee, however, is desirable as it allows the orienting of the orbit in such a way that the satellite can remain stationary for a long time over the night side of the Earth right after the terminator. Figure 8 to Figure 11 show the evolution over one year of a heliotropic orbit with the apogee on the night side. Due to the heliotropism condition, the relative angle between the apogee, the Earth and the Sun will remain almost constant during the year so that the SPS can always provide power to the night side. This particular

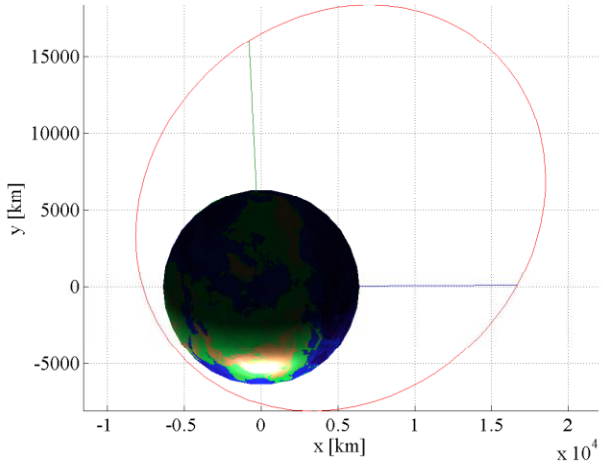

Figure 8. Example of heliotropic solution: winter solstice.

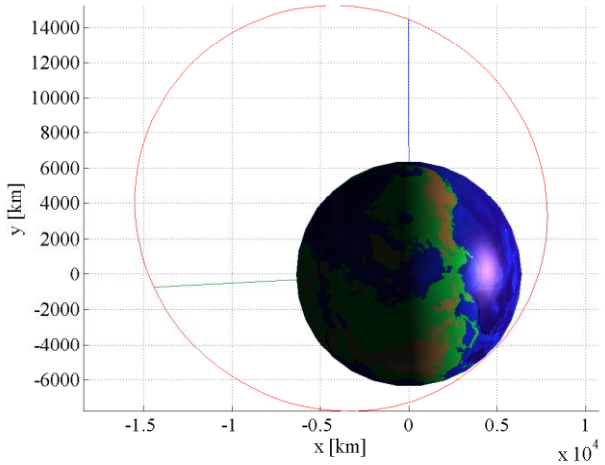

Figure 9. Example of heliotropic solution: spring equinox.

solution is prograde and has 1/5 resonance with the Earth, an inclination of 22.6° and a high altitude apogee that allows spending a long time in view of the night side. The time required to cover the area in between the green and blue radial lines in Figure 8 to Figure 11 is about 2.7 hours. Prograde solutions follow the ground station in its rotational motion. Furthermore, although the revisit time is 5 orbits, in this case it has to be noted that after a complete revolution, a bit more than 4.8 hours, the SPS can still see the ground station, though at a shallower elevation angle. In this way multiple stations can be served within one day and the same station can be in view twice within two full revolutions. It has to be noted however, that the heliotropism condition given in Eq. [10] involves both the right ascension of the ascending node and the argument of the perigee. Therefore, unless the critical inclination at 116.57° is considered, the argument of perigee will circulate. The consequence of this circulation is that the SPS will provide long term coverage to different regions during the year. Figure 12, Figure 14, Figure 16 and Figure 18 illustrate this seasonal coverage. Figure 12 shows that the areas in which the subsatellite point spends most of the time (circles with intense red colour) are north of the equator during the winter solstice. Figure 16 instead shows that for the same orbit the areas of longest persistence of the subsatellite point drift towards the southern hemisphere during the summer solstice.

At the critical inclination, the argument of perigee would not precess according to Eq. [9] and the apogee would cover always the same areas. However, the analysis in this paper is not sufficient to fully characterise the motion at the critical inclination and further analyses with a more complete model are required. Figure 13, Figure 15, Figure 17, Figure 19 show the Solar Aspect Angle (SAA) over one orbit period for the two solstices and the two equinoxes. The solar aspect angle is here defined as the angle between the satellite-earth vector and the satellite-Sun vector. When the satellite is an eclipse the SAA presents a gap.

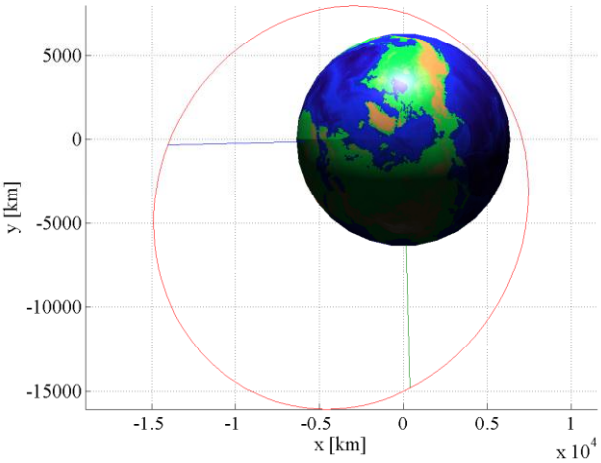

Figure 10. Example of heliotropic solution: summer solstice.

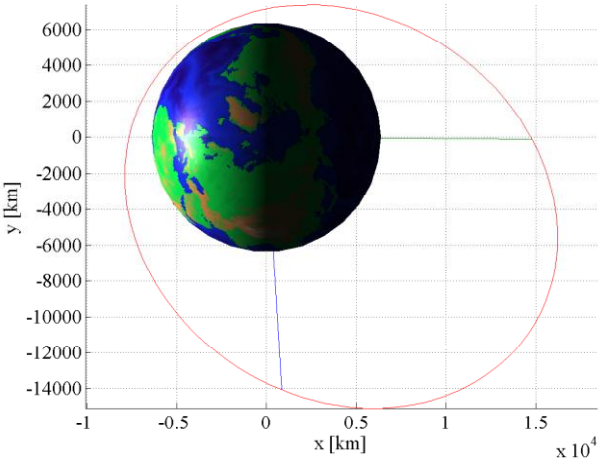

Figure 11. Example of heliotropic solution: autumn equinox.

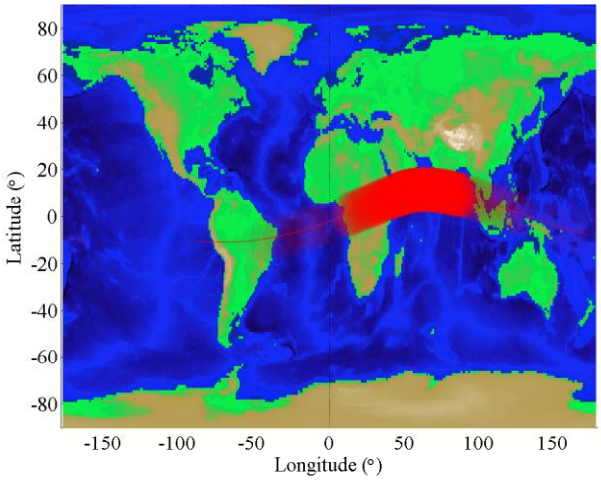

Figure 12. Coverage: Winter Solstice

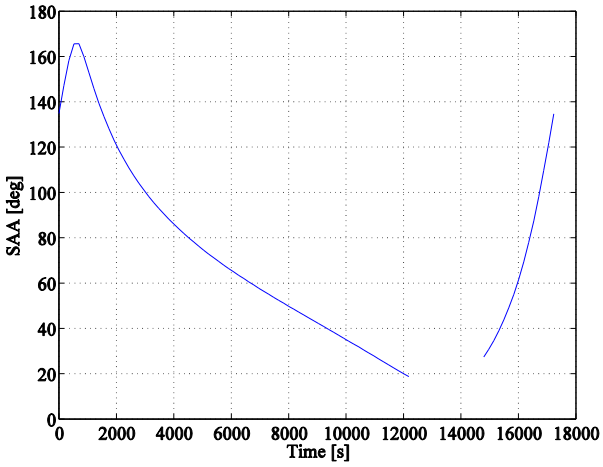

Figure 13. Solar aspect angle for the winter solstice

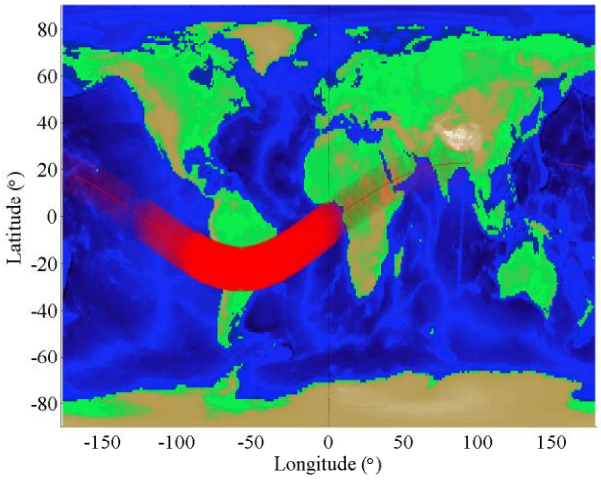

Figure 14. Coverage: Spring Equinox

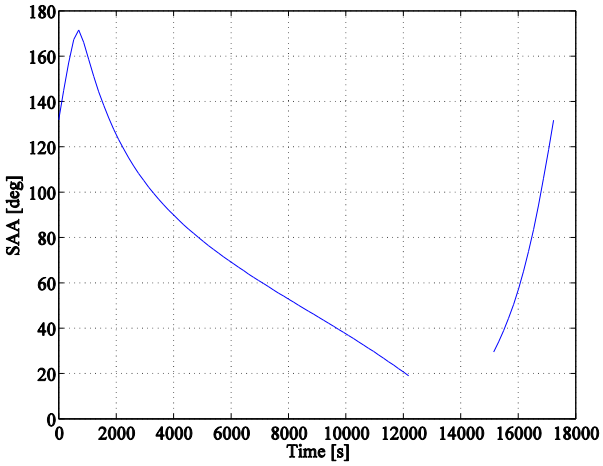

Figure 15. Solar aspect angle for the spring equinox

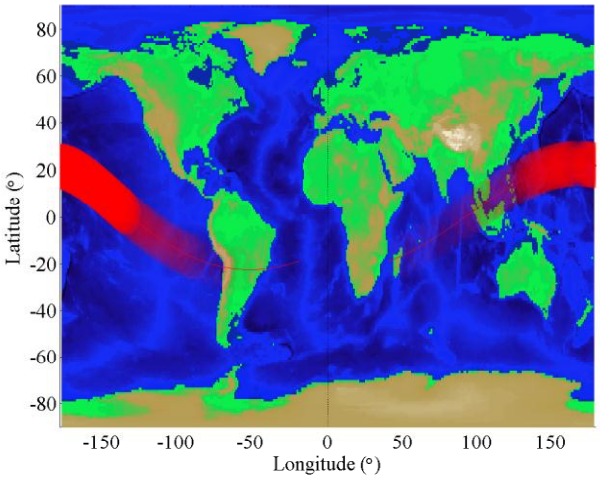

Figure 16. Coverage: Summer Solstice

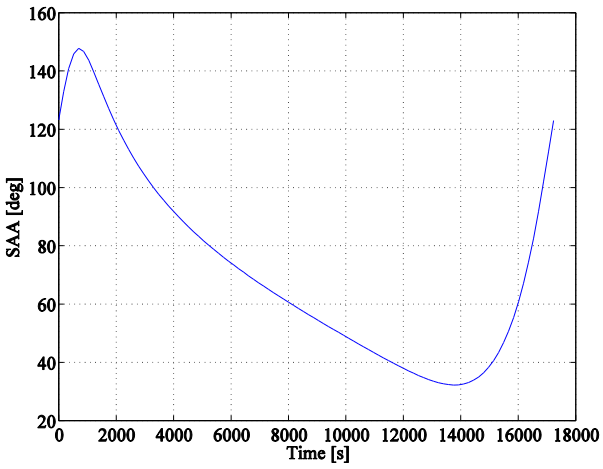

Figure 17. Solar aspect angle for the summer solstice solution

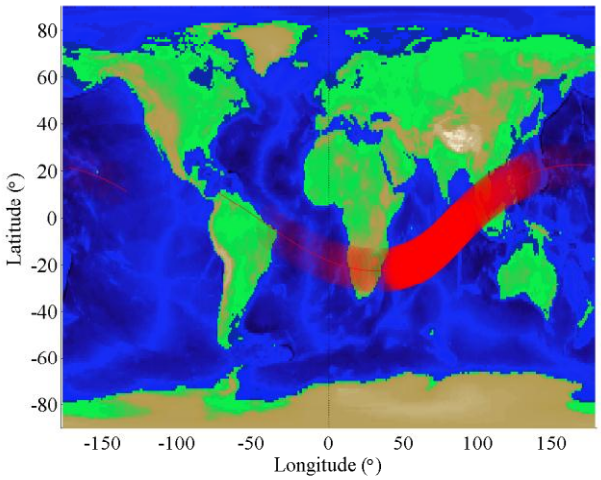

Figure 18. Coverage: Autumn Equinox.

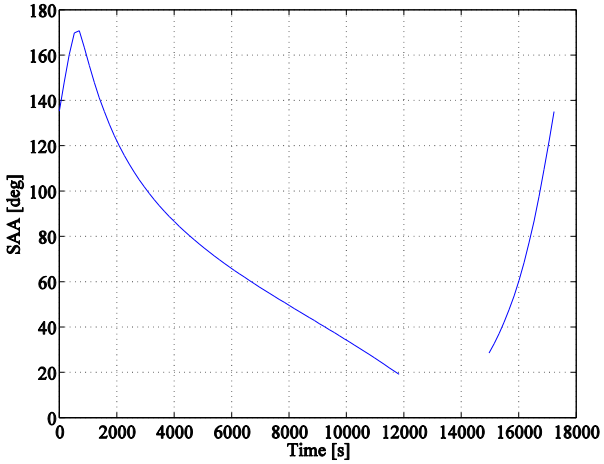

Figure 19. Solar aspect angle for the autumn equinox

The gap in these solutions, except for the solstice case that has no eclipse, is at an anomaly along the orbit of 225° (the green line in Figure 8 to Figure 11) and last for less than 40 minutes, therefore the longest contact period is spent with the satellite in sunlight and the ground station in shadow. By changing the initial right ascension, inclination and altitude one can minimise the period in eclipse.

An alternative to the use of heliotropic orbits would be to use frozen orbits (Molniya-like type of orbits) to maximise the time in view of the station. In this case, if only J_2 is considered, the following condition needs to be satisfied together with Eq.[14]:

$$\dot{\omega} = \frac{3nR_E^2 J_2}{4p^2}\left(4 - 5\sin^2 i\right) = 0 \qquad [15]$$

which is satisfied for the two critical inclinations at 63.435° and 116.57°. These orbit solutions provide repeated ground tracks with long contact time but $\dot{\Omega}$ precesses out of synch with respect to the Sun, therefore the satellites periodically sees the station during the day or during the night. Figure 20 shows the two critical inclinations and four families of orbits with a $\dot{\Omega}$ that is a fraction of the revolution period of the Earth. For a 1/1 resonance $\dot{\Omega} = \pm 2\pi / P_E$ with the plus sign corresponds to retrograde sun-synchronous orbits. It can be seen that there is an intersection between the critical inclination and sun-synchronous orbits through the altitude is relatively low. Furthermore, the orbit is retrograde which means that it would not follow the ground station. On the other hand, for a 1/2 resonance the altitude is significantly higher and would provide a periodic revisit of the northern hemisphere either in sunlight or in shadow.

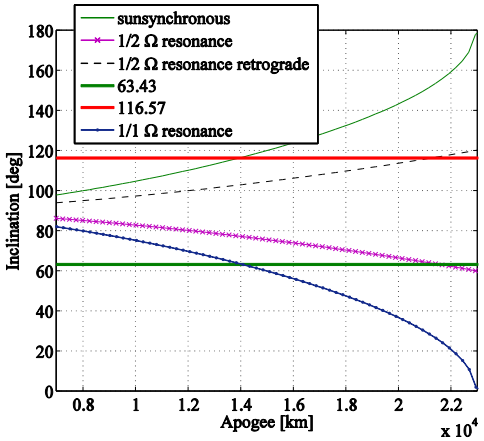

Figure 20. Ω resonant frozen orbits

A further possibility is represented in Figure 21 which is dual to the Ω-resonant solution. In this case, the spacecraft is placed on a sun-synchronous orbit and the altitude and inclination are tuned so that there is a resonance between the variation of ω and the revolution of the Earth. This corresponds to the satisfaction of the following two conditions:

$$\begin{aligned} &\frac{3nR_E^2 J_2}{4p^2}\left(4 - 5\sin^2 i\right) - \frac{k_2}{j_2}\frac{2\pi}{P_E} = 0 \\ &-\frac{3nR_E^2 J_2}{2p^2}\cos i - \frac{2\pi}{P_E} = 0 \end{aligned} \qquad [16]$$

with k_2 and j_2 two integer numbers.

For each intersection of the ω-resonant curves with the sun-synchronous curve there exists an orbit that has the orientation of the orbital plane that remains sun-synchronous but where the apogee circulates to periodically cover either the Northern or Southern hemisphere. For example for a 1/1 resonance the apogee can be placed at 46.4° North (133.6° inclination) on a dawn-dusk orbit in winter and the apogee will drift to the 46.4° South in summer. The main problem is that

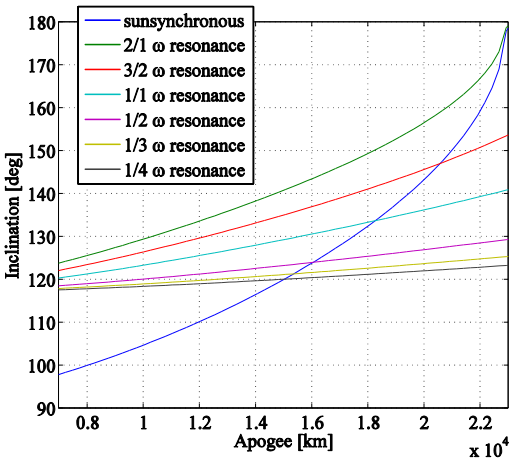

Figure 21. ω-resonant sun-synchronous orbits

due to the circulation of the argument of the perigee at the autumn equinox the satellite would see the ground station at dawn and not at dusk.

IV. PROXIMITY MOTION ANALYSIS

It is proposed to use a similar formation geometry for all three configurations of the disaggregated system. All of them, in fact, need to minimise the relative drift effect of J_2 and maximise the power generation and power delivery. In order to minimise the relative drift effect all satellites must be subject to the same $\dot{\Omega}$ and $\dot{\omega}$, therefore, from Eq. [8] and [9], the difference in inclination, semi-major axis and eccentricity must be zero. Under this condition and assuming a close formation with a relative distance between a few meters to a few tens of meters, the linear relative motion equations are[8]:

$$\begin{aligned}\delta x &= \frac{aesin(\theta+\omega)\delta M}{\eta}\\ \delta y &= \frac{r(1+ecos\theta)^2\delta M}{\eta^3} + r\delta\omega + r\cos i\delta\Omega\\ \delta z &= -rcos(\theta+\omega)\sin i\delta\Omega\end{aligned} \qquad [17]$$

where $\eta = \sqrt{1-e^2}$, $r = a(1-e^2)/(1+e\cos\theta)$ and $\delta M, \delta\omega, \delta\Omega$ are the differentials in mean anomaly, argument of the pericentre and right ascension of the ascending node. Given the proximity motion equations in Eq. [17], a constrained multi-objective optimisation can be formulated for the formation orbits that minimises the distance from the chief satellite (the master in the master-slave formation and the centre of the local relative coordinate system for the other two configurations) while minimising the interference. The problem can be formulated as follows:

$$\begin{aligned}&\min_{\delta M,\delta\omega,\delta\Omega}\ \max_{\theta}\ \delta r = \sqrt{\delta x^2+\delta y^2+\delta z^2}\\ &\max_{\delta M,\delta\omega,\delta\Omega}\ \min_{\theta}\ \sqrt{\delta x^2+\delta z^2}\\ &s.t.\\ &\min_{\theta}\delta y - \delta y_{\min} \le 0\end{aligned} \qquad [18]$$

where δy_{min} is negative in this example and the constraint on δy defines whether the cluster of satellites is flying ahead of the master or it is trailing. By solving problem [18] (we used an implementation Multiagent Collaborative Search for multiobjective optimisation problems[14]) one can find two families of symmetric orbits here called V-shape funnel orbits. A representation of the two families for different semi-major axis corresponding to Earth resonant chief orbits can be seen in Figure 22. The set of red dots corresponds to the resonance 1/10 in Figure 5 and the set of black dots to the resonance 1/5. The black set has

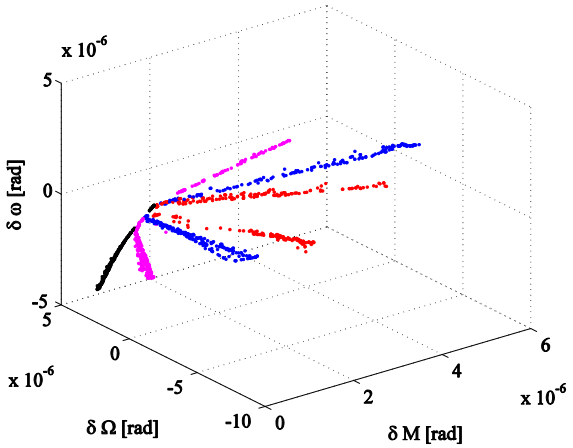

Figure 22. V-shape funnel orbit in the parameter space.

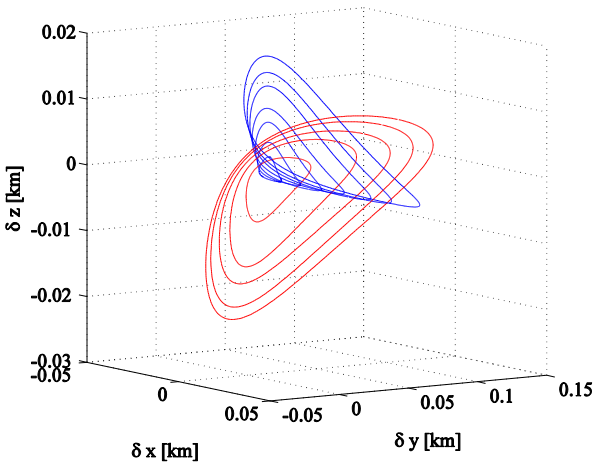

Figure 23. Example of V-shape funnel formation orbits

in fact two branches though only one is visible in the figure. Each branch of the V corresponds to a set of formation orbits with an opposite inclination with respect to the *x*-*y* plane. At the point in which each V is branching out, the two families of formation orbit coincide and correspond to a vertical formation orbit. Figure 23 shows an example of V-shape orbits for a 1/8 resonance heliotropic solution. The $\delta y_{\min}$ limit was set to 10 m to accommodate several satellites with minimum risk of impingement. From the results in Barker et al.[13] it is clear that at present near-field cannot extend to that distance. Although $\delta y_{\min}$ can be adjusted at will, the closer the formation orbit the smaller its size and the higher the risk of a collision.

V. CONCLUSIONS

This paper presented an analysis of a disaggregated system to beam energy from space to ground using lasers. The analysis considered several options for the operational orbit and formation configuration. The goal was to provide a limited amount of power in support of local users in different regions of the world. Some solutions offer a daily access to multiple users and a seasonal access to different parts of the world. These solutions can potentially be interesting both for fixed and mobile stations that require power during night time. A constellation of disaggregated systems would provide complete coverage to multiple users. It has to be noted that although the proposed solution employs lasers to beam energy, they can be equally good with microwave systems as the selection of the orbit is independent of the particular wireless transmission technology. On the other hand the current analysis considers only J_2 as the perturbing effect, thereby assuming that the solar pressure is negligible and higher harmonic effects are compensated. Future work will include other perturbations as they can be exploited to design other types of natural formations.

ACKNOWLEDGMENTS

The authors would like to thank Dr. David Burns and Dr. John-Mark Hopkins of the Institute of Photonics at Strathclyde University for their advice and suggestions on the laser sizing.

[1] Mankins, John C. (editor), Space Solar Power – Results of the First International Assessment, Cosmic Study Report from the International Academy of Astronautics, September 2011
[2] Kaya, N., "A new concept of SPS with a power generator/transmitter of a sandwich structure and a large solar collector," Space Energy and Transportation, Vol.1, No.3, pp.205-213, 1996
[3] Mankins J.C., Kaya N., Vasile M. SPS-ALPHA: The First Practical Solar Power Satellite via Arbitrarily Large Phased Array (A 2011-2012 NASA NIAC Project). AIAA IECEC 2012, Atlanta Georgia.
[4] Vasile .M., Maddock C.A. Design of a formation of solar pumped lasers for asteroid deflection. Advances in Space Research 50 (2012) 891–905.
[5] Summerer L., Purcell O., Concepts for Wireless Energy Transmission via Laser, IEEE ICSOS, 2009
[6] Midleton W.E.K., Vision Through the Atmosphere, University of Toronto Press, Toronto, 1952.
[7] Rubenchik A.M., Fedoruk M.P., Turitsyn S.K., Laser Beam Self-Focusing in the Atmosphere, Physical Review Letters, 102, 233902, 2009
[8] Schaub H., Junkins J.L. Analytical Mechanics of Space Systems, AIAA Education Series, 2003
[9] Vallado D.A. Fundamentals of Astrodynamics and Applications. Space Technology Libraries, 2007
[10] Krivov A.V., Sokolov L.L., Dikare V.V. Dynamics of Mars-Orbiting Dust: Effects of Light Pressure and Planetary Oblatness. Celestial Mechanics and Dynamical Astronomy, Vol. 63, No. 3, 1995, pp. 313-339. doi: 10.1007/bf00692293
[11] Hedman, M. M., Burt, J. A., Burns, J. A. and Tiscareno, M. S., "The Shape and Dynamics of a Heliotropic Dusty Ringlet in the Cassini Division," Icarus, Vol. 210, No. 1, 2010, pp. 284-297
[12] Colombo C., Lücking C., McInnes C.R.. Orbital dynamics of high area-to-mass ratio spacecraft with J2 and solar radiation pressure for novel Earth observation and communication services, International Astronautical Congress, Cape Town. IAC-11.C1.4.8., Acta Astronautica, DOI 10.1016/j.actaastro.2012.07.009
[13] Barker D., Summerer L., Assessment of near field wireless power transmission for fractionated spacecraft applications, 62nd International Astronautical Congress, Cape Town, South Africa, IAC-11-C3.2.7, 2011.
[14] Vasile M., Zuiani F. MACS: An Agent-Based Memetic Multiobjective Optimization Algorithm Applied to Space Trajectory Design. Institution of Mechanical Engineers, Part G, Journal of Aerospace Engineering, November 2011.
[15] nLIGHT, January, nLIGHT demonstrates 73% wall-plug efficiency. Press Release, 2006. http://www.nlight.net/news/releases.

[16] Peters, M., Rossin, V., Everett, M., Zucker, E., High-power, high efficiency laser diodes at JDSU. in: Proceedings SPIE 6456, 64560G, 2007.
[17] Jeong, Y., Sahu, J.K., Williams, R.B., Richardson, D.J., Furusawa, K., Nilsson, J. Ytterbium-doped large-core fibre laser with 272 w of output power. Electron. Lett. 39 (13), 977–978, 2003.
[18] Jeong, Y., Sahu, J.K., Baek, S., Alegria, C., Soh, D.B.S., Codemard, C., Nilsson, J. Cladding-pumped ytterbium-doped large-core fiber laser with 610 w of output power. Optics Commun. 234 (1–6), 315–319, 2004.
[19] Sabol, C., Draim, J. and Cefola, P., "Refinement of a Sun-Syncronous Critically Inclined Orbit for the Ellipso Personal Communication System," Journal of the Astronautical Sciences, Vol. 44, No. 4, 1996, pp. 467-489.
[20] Saikia T., Imasakia K., Motokoshia S., Yamanakaa C., Fujitab H., Nakatsukab M., Izawab Y. Disk-type Nd/Cr:YAG ceramic lasers pumped by arc-metal-halide-lamp. Optics Communications Volume 268, Issue 1, 1 December 2006, Pages 155–159.
[21] Larson, W. J. andWertz, J. R., Space Mission Analysis and Design, Microcosm Press and Kluwer Academic Publishers, 2005.